npj | Biofilms and Microbiomes

www.nature.com/npjbiofilms

ARTICLE OPEN

Check for updates

Attachment and antibiotic response of early-stage biofilms studied using resonant hyperspectral imaging

Yue Wang[1]✉, Christopher P. Reardon[1], Nicholas Read[2], Stephen Thorpe[2], Adrian Evans[3], Neil Todd[3], Marjan Van Der Woude[4] and Thomas F. Krauss[1]

Many bacterial species readily develop biofilms that act as a protective matrix against external challenge, e.g., from antimicrobial treatment. Therefore, biofilms are often responsible for persistent and recurring infections. Established methods for studying biofilms are either destructive or focus on the biofilm's surface. A non-destructive method that is sensitive to the underside of the biofilm is highly desirable, as it allows studying the penetration of antibiotics through the film. Here, we demonstrate that the high surface sensitivity of resonant hyperspectral imaging provides this capability. The method allows us to monitor the early stages of *Escherichia coli* biofilm formation, cell attachment and microcolony formation, in-situ and in real-time. We study the response of the biofilm to a number of different antibiotics and verify our observations using confocal microscopy. Based on this ability to closely monitor the surface-bound cells, resonant hyperspectral imaging gives new insights into the antimicrobial resistance of biofilms.

npj Biofilms and Microbiomes (2020)6:57 ; https://doi.org/10.1038/s41522-020-00169-1

INTRODUCTION

Biofilms are commonly defined as communities of surface-attached microorganisms embedded in an extracellular matrix that are attached to a surface. In most natural environments, polymicrobial biofilms are predominant and their survival often relies on intercellular communication and interactions[1,2]. In the last few decades, biofilms have attracted great attention in areas ranging from environmental studies to industrial water systems, from the food industry to chronic infections[3–6]. In fact, 60–80% of human bacterial infections, including many bloodstream and urinary tract infections, are caused by bacterial biofilms[7–10]. Biofilm-based infections are extremely difficult to cure, as biofilms are intrinsically much less susceptible to antimicrobial agents than non-adherent, planktonic cells. There are two main mechanisms for antimicrobial tolerance in biofilms. The first is the failure of an antimicrobial agent to diffuse and penetrate into the depth of the biofilm. This is due to the extracellular polymeric matrix that forms the biofilm and that is known to retard the diffusion of antimicrobial agents[11], and solutes in general. Hence the substratum, i.e., the surface-bound underside of the biofilm, remains protected. The second mechanism is that some of the biofilm cells experience nutrient limitation and, therefore, exist in a slow-growing or starved state[8–14]. Because of their much slower metabolism, slow-growing or non-growing cells are more tolerant of antimicrobial agents.

Recent studies have also shown that microorganisms growing in a biofilm are highly resistant to antimicrobial agents[15–19]. The antibiotic resistance in biofilms is generally caused by mutations and is driven by the repeated exposure of the bacteria to high levels of antibiotics as a consequence of treating the biofilm-associated infections, for instance[20,21]. The minimum inhibitory concentration (MIC), defined as the lowest concentration of an antimicrobial that will inhibit the visible growth of a microorganism, is often considered as the "gold standard" for determining the susceptibility of microorganisms to antimicrobials[22,23]. As a result from both biofilm tolerance and antimicrobial resistance, it is known that a subset of the sessile bacteria in biofilms can survive in the presence of up to 1000 times MIC, compared to the planktonic cells[24,25].

To account for this discrepancy, new pharmacodynamic parameters, such as the minimum biofilm inhibitory concentration (MBIC) and the minimum biofilm eradication concentration (MBEC) have been introduced. To evaluate antimicrobial activity on sessile bacteria, in-vitro systems with abiotic surfaces have been developed over the last decade[24–27]. Closed systems (batch culture), such as multi-well plate assays, the Calgary device, and open systems (continuous culture), such as substratum suspending reactors and the flow cell systems, are some of the most used in-vitro biofilm models for susceptibility studies[28], but they often require staining and/or dissolving the biofilms for visualisation and quantification, so they are typically destructive and do not allow monitoring the progression of antimicrobial activity.

Despite all of the advances made in biofilm antimicrobial resistance and tolerance studies, a highly sensitive system that is able to monitor biofilm formation and dispersion in real-time, non-destructively and quantitatively, is still missing. Monitoring the cell attachment and colonisation stage is paramount to this effort, as it allows for taking control of the early stages of biofilms and developing strategies for the prevention of mature biofilm formation. Similarly, monitoring the substratum of the biofilm is essential for understanding when antimicrobial action is completed. To address this challenge, we introduce the technique of resonant hyperspectral imaging to the monitoring of biofilms. We demonstrate the real-time monitoring of cell attachment and the development of micro-colonies of *Escherichia coli* (*E. coli*) bacteria on the sensor surface with a range of initial inoculum density, starting from 2×10^5 CFU per mL. Owing to the high surface sensitivity of the guided-mode resonance we employ, we are able to focus on the underside of the biofilm where antibiotic access is most challenging. We are able to provide a clear picture of the

[1]Department of Physics, University of York, Heslington, York, North Yorkshire YO10 5DD, UK. [2]Department of Biology, University of York, Heslington, York, North Yorkshire YO10 5DD, UK. [3]York Teaching Hospital NHS Foundation Trust, The York Hospital, York, North Yorkshire YO31 8HE, UK. [4]York Biomedical Research Institute, Hull York Medical School University of York, Heslington, York, North Yorkshire YO10 5DD, UK. ✉email: yue.wang@york.ac.uk

early-stage of biofilm formation and of the response of the biofilm to a range of antibiotics with varying doses. The unique information provided by resonant imaging may support the development of novel therapies for treating biofilm-associated infections.

RESULTS

Hyperspectral images of early-stage biofilms

The key element of our biofilm sensor is a grating that supports a guided-mode resonance (GMR)[29]. The grating is fabricated in a 150 nm thick silicon nitride (Si_3N_4) film on a glass substrate. Si_3N_4 has a high-refractive index to support the guided-mode, it exhibits minimal absorption at visible and near-infrared wavelengths, and most importantly, it is biocompatible, chemically inert and mechanically robust[30,31]. We first simulate the grating design using rigorous coupled-wave analysis (RCWA) and fabricate structures with a period of 569 nm and a filling factor (defined as the fraction of high-refractive index material in one period) of 80% for a resonance wavelength operating at 850 nm. The evanescent tail of the guided-mode extends beyond the grating layer and into the sensing region and thereby defines the detection volume. The size of the detection volume is determined by the difference between the effective index of the GMR and the refractive index of the sensing region, as is apparent from fundamental guided-mode theory[32]; the detection volume is typically 100–200 nm in depth and only extends into the first bacterial layer of the biofilm. Therefore, the sensor is able to monitor the very early stages of biofilm formation and the biofilm substratum, and is not susceptible to the background signal that arises from the bulk biofilm and the surrounding media.

Figure 1 is a schematic drawing of the experimental setup. The grating is placed into a flow cell to simulate the typical environment of interest, for instance a water pipe or the inside of the bladder, and to discourage settling of the bacteria. The flow is generated by a peristaltic pump with sterile silicone tubes. We used *E. coli* cultured in Luria-Bertani (LB) medium with an initial concentration of 2×10^8 CFU per mL and kept the bacteria in a

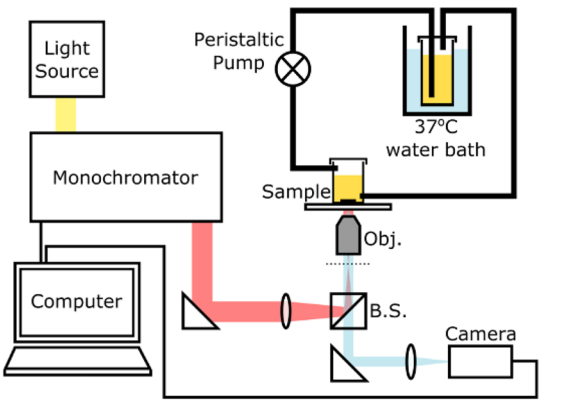

Fig. 1 Experimental setup. A broadband light source (SM30, Leukos) combined with a grating-based monochromator is employed to generate a single illumination wavelength with a spectral width of 0.6 nm, which is then guided into an inverted microscope with a 5x objective lens (Olympus NeoDplan). A GMR grating is mounted on the bottom of a flow cell with PDMS; the flow of *E. coli* culture is generated by a peristaltic pump with sterile silicone tubes from a reservoir of culture in a 37 °C water bath. The flow cell is used to avoid detection of the planktonic cells that happened to land on the grating but are not involved in biofilm formation. The camera used here is a CoolSnap Myo (Photometrics) with 970 x 730 pixels. Images are captured using LabView, and image analysis and curve fitting are performed using MATLAB.

37 °C water bath and flowed them through the sensor with a flow rate of 5 mL s^{-1}. Images from the sensor are formed hyperspectrally by taking a sequence of bright-field images that are typically obtained in less than 3 min depending on the camera's integration time (usually set to be 1 s) and the wavelength resolution (usually set to be 0.2 nm), each at a different illumination wavelength achieved via a tunable monochromatic light source. For example, it takes just over 2 min for a scan of 25 nm wavelength range with 0.2 nm resolution, i.e., 125 images, and a hyperspectral image of the resonance is then generated within seconds. By analysing the intensity values of each bright-field image, the resonance wavelength for each pixel can be determined. By plotting the resonance wavelengths of all pixels in the array, we produce the hyperspectral images of the grating at resonance (for example in Fig. 2(a–d)). The resulting hyperspectral image contains the spectral response at every pixel within the microscope's field of view. The region of interest (i.e., the centre of the GMR grating) consists of 200×200 pixels on the camera (corresponding to approximately $250 \times 250\ \mu m^2$ in size). We then combine the resonance wavelengths of all 200×200 pixels in each hyperspectral image as a histogram (see Fig. 2(e–h)), and by fitting a Gaussian curve to this histogram, we obtain a central resonance wavelength (λ_n) for each hyperspectral image. It is worth nothing here that the distribution in the resonant wavelengths at time 0, defined as λ_0, arises predominately from nanofabrication tolerances in a GMR grating. This uncertainty follows a normal distribution[33]; hence, a Gaussian distribution is used to determine the central resonant wavelength and the resonance uniformity. Finally, the shift in the central resonance wavelength ($\Delta\lambda = \lambda_n - \lambda_i$, while λ_i is defined as the base value of the resonance wavelength, averaged over the first 30 min after the flow of culture is started) caused by the refractive index change given by the bacterial attachment and the formation of micro-colonies, is plotted over time (see Fig. 2(i)). It appears that the shift in resonant wavelength, $\Delta\lambda$, saturates after ~5 h, which indicates that the first layer of the biofilm has been established (also see Supplementary Figs. 1 and 2); while it is understood that the biofilm continues to grow, the technique is not sensitive to further increases in thickness. We also note here that in the plane of the grating surface, the spatial resolution is 2 µm along the grating grooves and 6 µm in the direction perpendicular to the grating grooves[34].

Biofilm formation as a function of bacterial concentration

Cultures of *E. coli* were diluted to different concentrations, ranging from 2×10^5 to 2×10^8 CFU per mL. These dilutions were then used in separate experiments to inoculate the sensor and to study the rate of biofilm formation. We choose this range due to known clinical practice, where a specimen is considered positive for urinary tract infection in adults if the uropathogen concentration is $>10^5$ CFU per mL[35]. We then set the sensor to obtain a hyperspectral resonant image at intervals of 9 min. Figure 3(b–e) shows that resonance wavelength shift is characteristic of early-stage single species biofilm formation, which appears with a similar shape of typical growth curves of planktonic cells[36], although the mechanisms behind the curves are rather different. The biofilm formation profiles detected within a 15-h window can be described by three phases. Initially, planktonic bacteria attach to the surface —although some attachments are reversible (named "planktonic" phase). The attached cells then aggregate to form micro-colonies while excreting extracellular polymeric substances, making their attachment irreversible (named "colonies" phase). The bottom-layer of the biofilm is then considered established and continues to mature into a multi-layered cluster ("mature" phase). The "mature" phase, which can be upwards of multiple micrometres in thickness, is beyond the detection volume of our sensor and is, therefore, not "seen", hence the

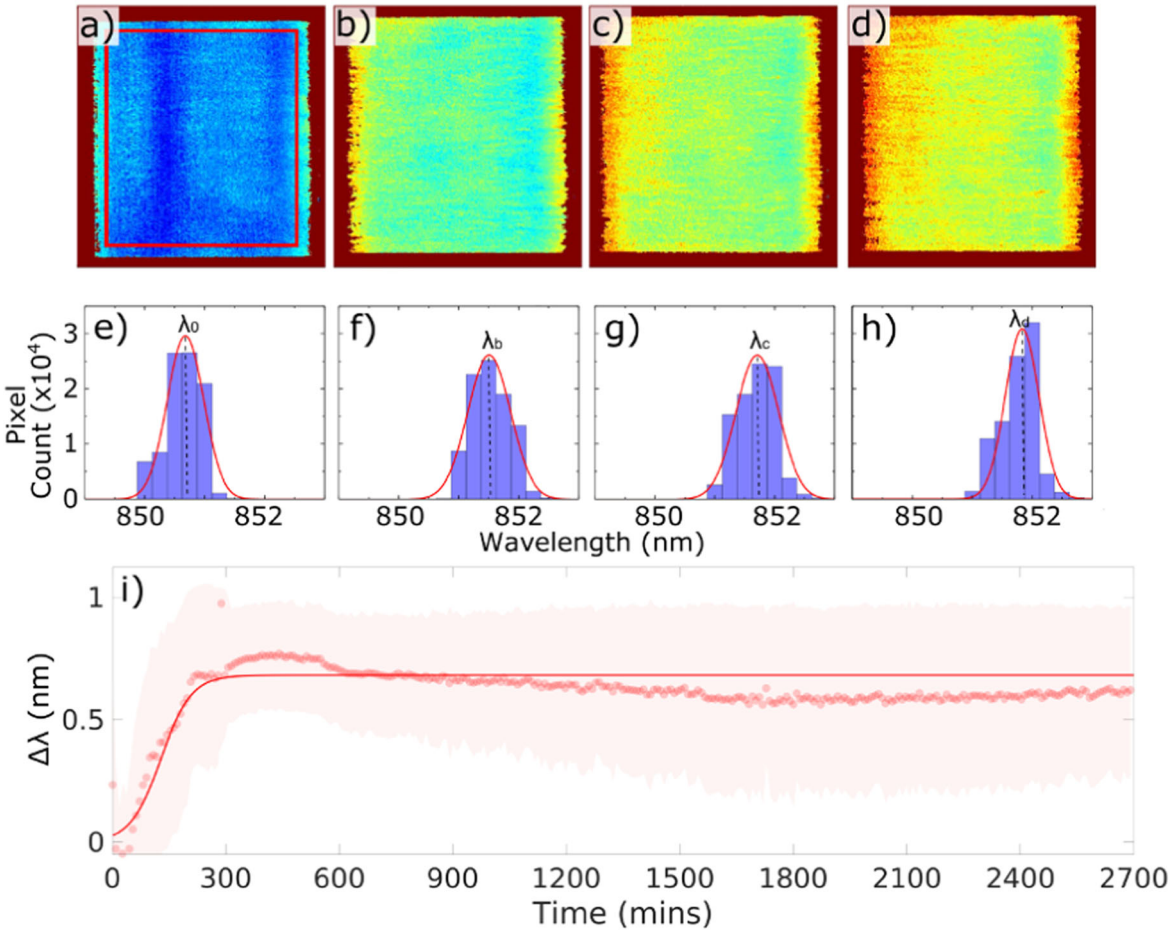

Fig. 2 Hyperspectral images and resonance wavelength shifts. a–d Hyperspectral images generated by the biofilm sensor at times 0, 2, 3.5 and 6 h from the start of the experiment. The colour represents the resonance wavelength; **e–h** histogram data of resonance wavelengths of all pixels in **a–d** correspondingly, and Gaussian fit (red curve) to determine the central wavelength: λ_0 (at 0 h), λ_b (at 2 h), λ_c (at 3.5 h) and λ_d (at 6 h); **i** plot of the resonance wavelength shift, $\Delta\lambda$ ($\Delta\lambda = \lambda_n - \lambda_i$), against time (dots represent the central resonance wavelength λ_n from each Gaussian fit; shaded areas illustrate standard deviations of corresponding Gaussian fits and delineates the distribution of the resonance wavelengths of all 200 x 200 pixels) and the solid line is a sigmoidal fit to the data. λ_i is defined as the base value of the resonance wavelength, averaged over the first 30 min after the flow of culture is started. Data showing long term (45 h) stability of the biofilm sensor with fresh LB media introduced into the flow cell at 24 h. The initial *E. coli* concentration used here is 2×10^8 CFU per mL.

resonance wavelength shift, Δλ, saturates. It is also known that the embedded biofilm cells do not divide and instead, their excess energy is used to maintain the extracellular matrix[11,37]. This explains why the resonance wavelength, i.e., the refractive index on the sensor surface, remains constant after a certain period of time.

A modified sigmoidal function is used to model the biofilm formation curves, see Fig. 3. As discussed above, the characteristic "S"-shaped biofilm formation curve appears similar to the typical shape of planktonic bacterial growth curve, where sigmoidal models, such as Gompertz model, are commonly employed in analysis[36,38]. Our modified sigmoidal function can be expressed in terms of the resonant wavelength shift, as follows:

$$\Delta\lambda = \frac{1}{1/A + \exp[-\alpha * (t - t_{\text{plank}})]}, \quad (1)$$

where A is the amplitude of the profile, t_{plank} is the time duration of the reversible cell attachment, which is indicated with a shaded region in Fig. 3, and α is the biofilm formation rate. The relationship between the bacterial seeding density and the "planktonic" phase time t_{plank} is discussed in Supplementary Information (see Supplementary Fig. 3). Although it is intuitive that a higher initial inoculum density leads to a shorter biofilm formation time, the technique readily allows us to quantify this formation time. More importantly, the technique allows us to quantify the biofilm's response to antibiotics, as discussed in the next section.

Response of *E. coli* biofilms to antibiotics

Next, we use the sensor to study the response of biofilms to antibiotic challenge, especially the response of the cells at the bottom-layer of the biofilm. With monitoring the changes on the grating surface, we aim to detect which antibiotic can effectively disrupt the biofilm substratum. If the antibiotic causes a disruption to the distribution of the biofilm substratum, or partial or full detachment of the biofilm, we should observe a change in resonance wavelength of the grating. We use a concentration of 2×10^8 CFU per mL in order to speed up the process; using this concentration, the bottom-layer of the biofilm is typically established within 5–6 h (see Supplementary Fig. 1 and 2). Our real-time, non-destructive monitoring capability then allows us to introduce antibiotics before, during and after a biofilm has been formed on the sensor surface.

For uncomplicated lower urinary tract infections in adults, current UK NICE (The National Institute for Health and Care Excellence) guidelines recommend nitrofurantoin (which inhibits the citric acid cycle, as well as synthesis of DNA, RNA, and protein,

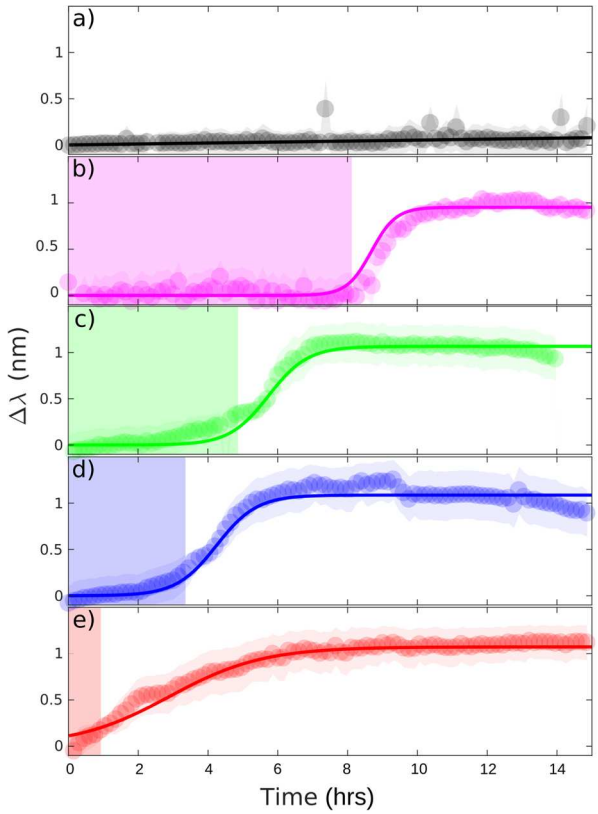

Fig. 3 Biofilm formation time as a function of *E. coli* concentration. a LB broth only, for reference. Concentrations of (**b**) 2×10^5, (**c**) 2×10^6, (**d**) 2×10^7, (**e**) 2×10^8 CFU per mL in LB. At least three independent replicates were performed for each concentration and reference. The solid lines are sigmoidal fits to the data and the fitting parameters are presented in Table 1. The shaded region indicates the duration of the reversible cell attachment, t_{plank}.

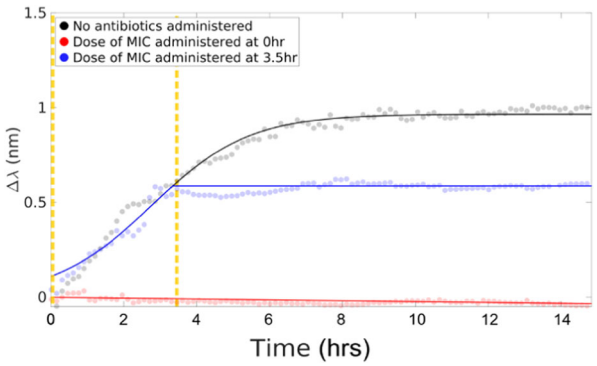

Fig. 4 Antimicrobial susceptibility testing in early-stage biofilms. A 1x MIC dose of trimethoprim is introduced to the culture at 0 h and at 3.5 h (as indicated by the vertical dashed lines). The solid black line is a sigmoidal fit to the data. After introducing the antibiotic, the data are fit to a straight line.

also a bactericidal antibiotic) and trimethoprim (a folic acid synthesis inhibitor, a bacteriostatic antibiotic) as first line antibiotics due to their low risk of microbial resistance[39]. We, therefore, choose these two drugs as our model antibiotics. The MIC and the minimum bactericidal concentration (MBC) were pre-assayed with planktonic *E. coli* cells in 96-well plates (see Supplementary Information and Supplementary Fig. 4 for details). The MIC of trimethoprim for this strain is determined to be < 1 μg mL^{-1} and the MBC as 16–32 μg mL^{-1}. Trimethoprim with a dose of 1 μg mL^{-1} is, therefore, introduced into the culture at times 0, 3.5 and 5.0 h. We make the following observations (Fig. 4):

- When the antibiotic is injected at time 0 h, it completely halts cell attachments, and no colonisation and subsequent multi-layered biofilm formation is observed on the sensor surface;
- When the antibiotic is added at 3.5 h, the colonies stop developing immediately upon introduction of the drug, halting any further establishment of the biofilm;
- When 1x MIC of trimethoprim is added at 5.0 h (after the profile shows "saturation"), there is no observable change, i.e., the curve looks identical to the one without antibiotics added (see Supplementary Information). This indicates that there is no change, i.e., in terms of colony density or detachment, at the bottom-layer of the biofilm.

In order to study the biofilm tolerance, we increase the dose of trimethoprim from 1 to 500x MIC (equivalent to 20x MBC approximately). The antibiotic solutions are administrated at 5 h from the start of the experiments, i.e. after the monolayer of biofilm is established. There is no significant effect on the detected resonance wavelength at any dose (see Fig. 5(a) for 500x MIC and more details in Supplementary Fig. 5). As the sensor probes the substratum of the biofilm, i.e., the volume that is in direct contact with the grating, the results indicate that even with extremely high doses of trimethoprim, the sensor does not detect significant changes. A separate study on nitrofurantoin reveals very similar results to trimethoprim (see Supplementary Fig. 6 for more information). We can, therefore, conclude that nitrofurantoin and trimethoprim are effective against planktonic cells, but not against biofilms formed by the same strain.

Confocal fluorescence microscope images confirm our findings (Fig. 5b, c, g, h). Following the addition of 500x MIC of trimethoprim, introduced to the culture at 5 h, the biofilm is allowed to continue "growing" for at least a further 5 h with the antibiotic present. We observe that there is still a good bacterial coverage on the grating after the multiple wash steps that are required during the staining process, and the majority of cells attached to the surface are still alive (Fig. 5c, and more confocal fluorescence images in Supplementary Fig. 7). This confirms that the bottom-layer of the biofilm is undisrupted, in agreement with our sensor result. As clearly observed in Fig. 5(c), there are too many surviving bacteria in the 500x MIC case that remain attached to the sensor surface to consider this a biofilm eradication concentration (MBEC). This observation indicates that the MBEC is higher than 500x MIC, i.e., 0.5 mg mL^{-1} in this case, which is also consistent with other reports employing fluorescent testing methods[24,25]. Colony counting on agar plates after 24 h incubation revealed that there are living cells in the remaining biofilms.

So our recognition that trimethoprim is not effective against biofilms is confirmed by multiple control methods.

We then tested two other bactericidal antibiotics, i.e., rifampicin (an RNA synthesis inhibitor, can be bacteriostatic or bactericidal depending on concentrations) and ciprofloxacin (inhibits DNA replication and exhibits both bacteriostatic and bactericidal activities), and they have been suggested because of their efficacy against biofilms. Identifying the best antimicrobials against biofilms is an active area of research[13,40,41] that may benefit from a simple and real-time, non-destructive technique such as ours.

With our biofilm sensor, the disruption at the bottom of biofilm is observed as a shift of the resonance wavelength shortly after the administration of ciprofloxacin to a biofilm after 5 h of growth (Fig. 5(f)). Confocal microscopy with the live/dead assay confirms that the coverage of bacteria on the sensor surface is significantly reduced, and the cells in one remaining colony attached to the surface are also mostly dead (red colour) or injured with compromised cell membranes (yellow colour), shown in Fig. 5 (h). This outcome is significantly different to what we observe with the other antibiotics, even though the phase contrast images of all

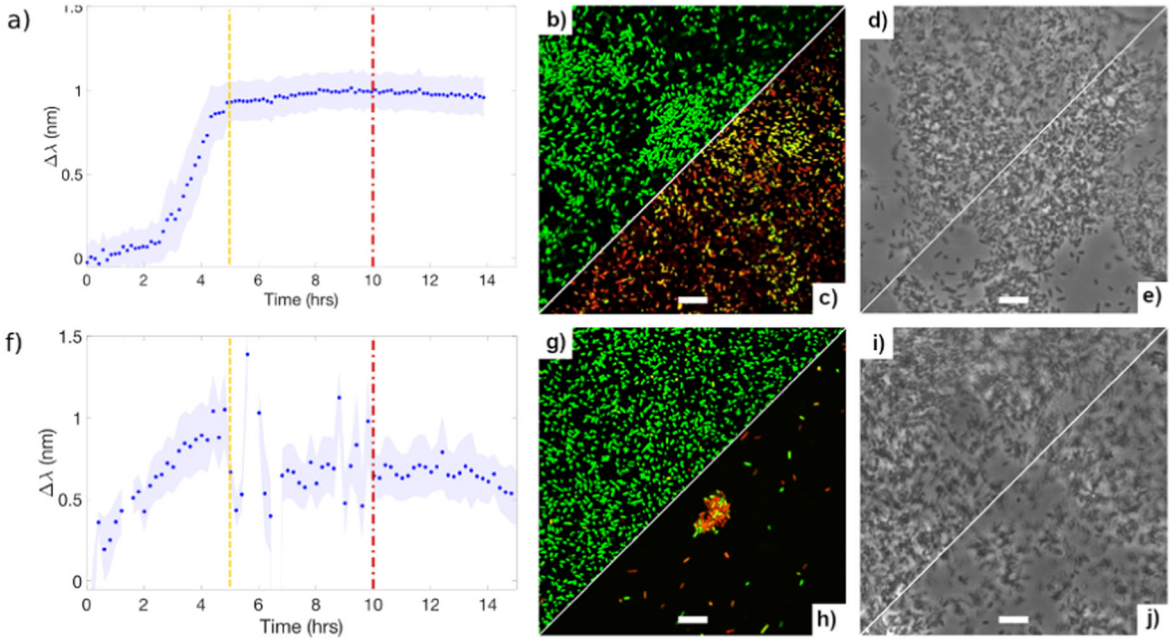

Fig. 5 Three different techniques to monitor biofilms: GMR sensor (left), confocal fluorescence microscope (middle), and phase contrast microscope (right). Trimethoprim (final dose of 500x MIC, **a**–**e**) and ciprofloxacin (final dose of 300x MIC, **f**–**j**) injected at 5 h (dashed line) from the beginning of the experiment and microscopic images are obtained after 10 h (dash dotted line) from the start of the experiments. Confocal microscopic images (**b**, **c** and **g**, **h**) and phase contrast images (**d**, **e** and **i**, **j**) are all taken at 10 h from the start of the experiments; **c** and **h**, **e** and **j** are confocal and phase contrast images of biofilms with antibiotic injected at 5 h from the start of the experiments, respectively; The scale bars in the micrographs are all 10 μm long.

these samples are rather similar (Fig. 5d–e and i–j). The phase contrast images include not only the cells attached to the surface, but also the biofilm cells that are detached from the surface but near the surface, as well as some planktonic cells. In contrast, confocal microscopy with the Live/Dead staining involves a few washing steps during the process (see "Methods"), therefore, the confocal images represent the biofilm cells that are still firmly attached to the sensor surface. In Fig. 5f, it certainly appears that 300x MIC ciprofloxacin results in a rapid and significant disruption on the bottom of the biofilm. Indeed, this disruption seems to cease after 5 h and our hypothesis is that ciprofloxacin causes removal of majority of the biofilm on the sensor surface, leaving a small number of cells possibly with some exocellular matrix remaining on the surface, which is reflected by a small resonance wavelength shift after 10 h in Fig. 5(f). In short, our GMR sensor, compared to the conventional microscopic techniques, provides a non-destructive, rapid, dynamic sensing and analysis technique, which can provide real-time information of the very bottom of biofilm.

For ease of comparison and reproducibility, all of these studies have been performed in LB broth and each set of experiments has been repeated for a minimum of three times. We have also performed total biofilm removal experiments with 70% ethanol wash followed by a piranha etch (a 3:1 mixture of sulfuric acid and 30% hydrogen peroxide). This protocol removes any organic residues on the grating surface including the extracellular matrix. A total recovery of the original resonance wavelength is observed, which indicates that complete removal of biofilms can be detected by our sensor. To ensure clinical relevance, we have also demonstrated that the technique is compatible with undiluted human urine (see Supplementary Fig. 8).

DISCUSSION

In summary, we have introduced the technique of resonant hyperspectral imaging to monitoring the formation of *Escherichia coli* biofilms and have studied the response of these biofilms to a range of antibiotics. The key aspect that makes the technique so suitable for studying biofilms is that it only images the first few 100 nm from the bottom, i.e., the substratum, of the biofilm, which is the most important section of the film in terms of both early formation and antibiotic challenge. As the technique is only sensitive to the substratum, the sensing signal is not affected by the media, the thickness of the biofilm or to any planktonic cells suspended in the media, so it is easy to achieve a high signal to noise ratio. Furthermore, within the same assay, a quantitative indication of the bacteria concentration can be readily obtained by monitoring the time it takes for the onset of biofilm formation. Given this real-time monitoring capability, the technique also allows antimicrobial resistance testing in-situ, therefore offering the opportunity of quantitatively analysing the action and progression of different antibiotics against the biofilm within minutes to a few hours. The non-destructive nature of the technique is a unique advantage, compared to, e.g., fluorescence-based microscopy techniques.

We envisage that our system can be miniaturised into a hand-held device that could be implemented as a diagnostic within a clinical environment; such a realisation would allow for, e.g., the tailoring of antibiotic therapies to individual patients. Alternatively, the technique could be used for in-field biofilm detection, such as within water treatment plants or domestic water delivery pipes, food processing plants and equipment, heating, ventilation, and air-conditioning (HVAC) systems etc.. One can also envisage further improvements in terms of response time by accelerating bacterial attachment by using antibodies or carbohydrate coatings such as mannose. Undoubtedly, in a real biological or industrial system, the environment is far more complicated and polymicrobial biofilms tend to dominate. Although the polymicrobial nature of biofilms would not limit the performance of our sensor, additional sample or surface treatments may be used with our sensing system in order to improve specificity. For instance, pre-filtering or surface functionalisation could be employed in biofilm

Table 1. List of fitting parameters in Fig. 3, with the R^2 value for each fit.

Initial concentration [CFU per mL]	A [nm]	t_{plank} [h]	α [nm per h]	R^2
2×10^5	0.952	8.22	0.428	0.92
2×10^6	1.07	4.93	0.267	0.94
2×10^7	1.09	3.40	0.260	0.96
2×10^8	1.07	0.94	0.112	0.97

related bloodstream infection studies in order to gain some insight on the roles of each species in a biofilm community. Reports have also shown that the growth dynamics of a polymicrobial biofilm involve some extra phases[42], which can be further explored using our sensor system in future work.

Overall, we believe that our technique may be widely applicable both in industry and healthcare for fundamental studies and for applications that require the detection and monitoring of biofilms. With its high sensitivity to any changes in the substratum of biofilms, our sensor can be used in conjunction with other conventional techniques in order to gain a comprehensive understanding of biofilm formation, tolerance and antimicrobial resistance.

METHODS

Bacterial strain and growth conditions

E. coli K-12 carrying the F conjugative plasmid, also known as *E. coli* TG1, is chosen in this work as it has been shown previously to promote thick, mature biofilms within a short period of time[43,44]. A single colony is inoculated into a test tube containing 25 mL of liquid Luria-Bertani (LB) broth and placed in an orbital rotating shaker at 4 x *g* overnight at 37 °C. Some of this culture is then transferred and diluted within a fresh tube of LB broth to obtain the required concentrations of the microbial suspension. Optical density (OD) measurements are performed alongside separate cell counting on LB agar plates to determine bacterial concentrations. For example, $OD_{600nm} = 0.2$ corresponds to a 2×10^8 CFU per mL concentration.

Fabrication of resonance gratings and flow cell

In order to fabricate the gratings, a 150 nm Si_3N_4-on-glass substrate is cleaned in a piranha solution (hydrogen peroxide: sulfuric acid = 1:3 ratio), rinsed in acetone and isopropanol, and dried with nitrogen. The substrate is then coated with e-beam resist (ARP-13, AllResist GmbH), spun at 280 x *g* for 60 s, and baked at 180 °C for 10 min, resulting in a film of approximately 400 nm. For charge dissipation during e-beam exposure, a thin film of aluminium (20 nm) is deposited on top of the resist using a thermal evaporator (HEX, Mantis). The grating pattern is defined in the e-beam resist using an electron beam lithography system (Raith GmbH Voyager 50 kV), followed by pattern transfer into the substrate using reactive ion etching with a gas mixture of CHF_3 and O_2. The depth of the grating in the substrate is 150 nm. The aluminium layer is removed in phosphoric acid and the residue of e-beam resist is removed with Microposit resist remover 1165 (MicroChem). The fabricated grating is then fixed to the bottom of a sterile quartz glass container. The flow of *E. coli* culture is generated by a peristaltic pump with sterile silicone tubes from a reservoir of culture, typically a total of 40 mL, in a 37 °C water bath. Each set of experiments (including each *E. coli* concentration, references, each antibiotic and different concentrations) were repeated a minimum of three independent times.

Live/dead staining and confocal microscopy

After a certain time of growth, the grating is taken out from the flow cell, gently washed with phosphate buffered saline (PBS) buffer (Sigma-Aldrich) three times to remove the remains of the medium and planktonic cells, as well as loosely attached non-biofilm cells, and then incubated for 15 min in the dark with the BacLight Live/Dead viability kit (Thermo Fisher Scientific) to stain the cells with two fluorescent dyes, SYTO® 9 (green) and propidium iodide (red). Samples were then rinsed twice with PBS buffer and sealed under a coverslip. The stained biofilms on the grating are visualised using a ZEISS LSM 880 Confocal Microscope with a plan apochromat 63x oil-immersion objective. The Live/Dead viability kit stains live cells green, dead cells red and some cells appear yellow or orange indicating that those bacteria are injured with possibly compromised cell membranes[45].

Antibiotic preparation and MIC assay

Stock solution of 10 mg mL^{-1} of four antibiotics, i.e. trimethoprim, nitrofurantoin, rifampicin and ciprofloxacin (Sigma-Aldrich), are prepared by dissolving in dimethyl sulfoxide, diluting in deionized water and filter sterilising (0.22 µm syringe filter, Fisher Scientific). A microdilution assay was also performed on 96-well plates by exposing *E. coli* TG1 to a serial dilution of trimethoprim, nitrofurantoin, rifampicin and ciprofloxacin, in order to determine the MIC of each drug. The reporter dye resazurin was added to indicate the viability status of the cells[46]. For more details on the protocol, see Supplementary Information. The MIC measurements were performed with OD = 0.2, i.e., 2×10^8 CFU mL^{-1}, and repeated for four times.

Bacteria-spiked urine sample

For the bacteria-spiked urine sample shown in Supplementary Information, an overnight-grown suspension of *E. coli* cells in LB broth is centrifuged at 14,000 x *g* for 10 min, and washed in syringe-filtered human urine (0.22 µm filter, Fisher Scientific). This process is repeated three times. Then the *E. coli* cells are resuspended in syringe-filtered human urine and the final concentration is made to be 2×10^8 CFU per mL in urine.

Reporting summary

Further information on research design is available in the Nature Research Reporting Summary linked to this article.

DATA AVAILABILITY

The authors declare that all the data supporting the findings of this study are available within the article and the Supplementary Information file, or upon request from the corresponding author.

CODE AVAILABILITY

The authors declare that all the MATLAB code supporting the findings of this study are available upon request from the corresponding author.

Received: 9 March 2020; Accepted: 30 October 2020;
Published online: 27 November 2020

REFERENCES

1. Jabra-Rizk, M. A. Pathogenesis of polymicrobial biofilms. *Open Mycol. J.* **5**, 39–43 (2011).
2. Willems, H., Xu, Z. & Peters, B. M. Polymicrobial biofilm studies: from basic science to biofilm control. *Curr. Oral. Health Rep.* **3**, 36–44 (2016).
3. Hall-Stoodley, L., Costerton, J. W. & Stoodley, P. Bacterial biofilms: from the natural environment to infectious diseases. *Nat. Rev. Microbiol.* **2**, 95–108 (2004).
4. Stoodley, P. et al. Biofilms as complex differentiated communities. *Annu. Rev. Microbiol.* **56**, 187–209 (2002).
5. Van Houdt, R. & Michiels, C. W. Biofilm formation and the food industry, a focus on the bacterial outer surface. *J. Appl. Microbiol.* **109**, 1117–1131 (2010).
6. Parsek, M. R. & Singh, P. K. Bacterial biofilms: an emerging link to disease pathogenesis. *Annu. Rev. Microbiol.* **57**, 677–701 (2003).
7. Curtis Nickel, J. et al. Bacterial biofilms: influence on the pathogenesis, diagnosis and treatment of urinary tract infections. *J. Antimicrob. Chemother.* **33**, 31–41 (1994).
8. Costerton, J. W., Stewart, P. S. & Greenberg, E. P. Bacterial biofilms: a common cause of persistent infections. *Science* **284**, 1318–1322 (1999).
9. Anderson, G. G. et al. Intracellular bacterial biofilm-like pods in urinary tract infections. *Science* **301**, 105–107 (2003).
10. Trautner, B. W. & Darouiche, R. O. Role of biofilm in catheter-associated urinary tract infection. *Am. J. Infect. Control.* **32**, 177–183 (2004).

11. Branda, S. S. et al. Biofilms: the matrix revisited. *Trends Microbiol.* **13**, 20–26 (2005).
12. Pamp, S. J. et al. Tolerance to the antimicrobial peptide colistin in *Pseudomonas aeruginosa* biofilms is linked to metabolically active cells, and depends on the pmr and mexAB-oprM genes. *Mol. Microbiol.* **68**, 223–240 (2008).
13. Conlon, B. P. et al. Activated ClpP kills persisters and eradicates a chronic biofilm infection. *Nature* **503**, 365–370 (2013).
14. Lewis, K. Riddle of biofilm resistance. *Antimicrob. Agents Chemother.* **45**, 999–1007 (2001).
15. Donlan, R. M. Biofilms and device-associated infections. *Emerg. Infect. Dis.* **7**, 277–281 (2001).
16. Mah, T. F. & O'Toole, G. A. Mechanisms of biofilm resistance to antimicrobial agents. *Trends Microbiol.* **9**, 34–39 (2001).
17. Donlan, R. M. & Costerton, J. W. Biofilms: survival mechanisms of clinically relevant microorganisms. *Clin. Microbiol. Rev.* **15**, 167–193 (2002).
18. Hall-Stoodley, L. et al. Towards diagnostic guidelines for biofilm-associated infections. *FEMS Immunol. Med. Microbiol.* **65**, 127–145 (2012).
19. Davies, D. Understanding biofilm resistance to antibacterial agents. *Nat. Rev. Drug Discov.* **2**, 114–122 (2003).
20. Ciofu, O. & Tolker-Nielsen, T. Tolerance and Resistance of *Pseudomonas aeruginosa* biofilms to antimicrobial agents-how *P. aeruginosa* can escape antibiotics. *Front. Microbiol.* **10**, 913 (2019).
21. Bowler, P. G. Antibiotic resistance and biofilm tolerance: a combined threat in the treatment of chronic infections. *J. Wound Care* **27**, 5 (2018).
22. Andrews, J. M. Determination of minimum inhibitory concentrations. *J. Antimicrob. Chemother.* **48**, 5–16 (2001).
23. Wiegand, I. et al. Agar and broth dilution methods to determine the minimal inhibitory concentration (MIC) of antimicrobial substances. *Nat. Protoc.* **3**, 163–175 (2008).
24. Macià, M. D., Rojo-Molinero, E. & Oliver, A. Antimicrobial susceptibility testing in biofilm-growing bacteria. *Clin. Microbiol. Infect.* **20**, 981–990 (2014).
25. Olson, M. E. et al. Biofilm bacteria: formation and comparative susceptibility to antibiotics. *Can. J. Vet. Res.* **66**, 86–92 (2002).
26. Gordon, V. D. et al. Biofilms and mechanics: a review of experimental techniques and findings. *J. Phys. D: Appl. Phys.* **50**, 223002 (2017).
27. Kasimanickam, R. K. et al. Prevention and treatment of biofilms by hybrid- and nanotechnologies. *Int. J. Nanomed.* **8**, 2809–2819 (2013).
28. Ceri, H. et al. The calgary biofilm device: new technology for rapid determination of antibiotic susceptibilities of bacterial biofilms. *J. Clin. Microbiol.* **37**, 1771–1776 (1999).
29. Triggs, G. J. et al. Chirped guided-mode resonance biosensor. *Optica* **4**, 229–234 (2017).
30. Petzow, G., Herrmann, M. & Janson, M. High performance non-oxide ceramics II (structure and bonding). *Springe.-Verl.* **102**, 47 (2002).
31. Bal, B. S. & Rahaman, M. N. Orthopedic applications of silicon nitride ceramics. *Acta Biomaterialia* **8**, 2889–2898 (2012).
32. Yariv, A. Coupled-wave theory for guided-wave optics. *IEEE J. Quant. Electron.* **QE-9**, 919–933 (1973).
33. Fan, W. et al. Influence of fabrication error on the characteristics of a 2-D photonic-crystal cavity. *J. Lightwave Technol.* **28**, 1455–1458 (2010).
34. Pitruzzello, G. & Krauss, T. F. Photonic crystal resonances for sensing and imaging. *J. Opt.* **20**, 073004 (2018).
35. Franz, M. & Hörl, W. H. Common errors in diagnosis and management of urinary tract infection. I: Pathophysiology and diagnostic techniques. *Nephrol. Dial. Transplant.* **14**, 2746–2753 (1999).
36. Wang, L. et al. Bacterial growth, detachment and cell size control on polyethylene terephthalate surfaces. *Sci. Rep.* **5**, 15159 (2015).
37. Sutherland, I. W. The biofilm matrix–an immobilized but dynamic microbial environment. *Trends Microbiol.* **9**, 222–227 (2001).
38. Zwietering, M. H. et al. Modeling of the bacterial growth curve. *Appl. Environ.* **56**, 1875–1881 (1990).
39. *Urinary tract infection (lower): antimicrobial prescribing, NICE guideline link:* https://bnf.nice.org.uk/treatment-summary/urinary-tract-infections.html.
40. Coulter, L. B. et al. Effect of bacteriophage infection in combination with tobramycin on the emergence of resistance in *Escherichia coli* and *Pseudomonas aeruginosa* biofilms. *Viruses* **6**, 3778–3786 (2014).
41. Ravn, C. et al. Reduced ability to detect surface-related biofilm bacteria after antibiotic exposure under in vitro conditions. *Acta Orthopaedica* **87**, 644–650 (2016).
42. Fischer, M., Friedrichs, G. & Lachnitd, T. Fluorescence-based quasicontinuous and in situ monitoring of biofilm formation dynamics in natural marine environments. *Appl. Environ. Microbiol.* **80**, 3721–3728 (2014).
43. Ghigo, J. Natural conjugative plasmids induce bacterial biofilm development. *Nature* **412**, 442–445 (2001).
44. Reisner, A. et al. Development and maturation of *Escherichia coli* K-12 biofilms. *Mol. Microbiol.* **48**, 933–946 (2003).
45. Privat-Maldonado, A. et al. Nontarget biomolecules alter macromolecular changes induced by bactericidal low–temperature plasma. *IEEE TRPMS* **2**, 121–128 (2018).
46. Sarker, S. D., Nahar, L. & Kumarasamy, Y. Microtitre plate-based antibacterial assay incorporating resazurin as an indicator of cell growth, and its application in the in vitro antibacterial screening of phytochemicals. *Methods* **42**, 321–324 (2007).

ACKNOWLEDGEMENTS

We acknowledge financial support by the EPSRC of the UK (Grants EP/P02324X/1 and EP/P030017/1). Prof Thomas F. Krauss acknowledges a Royal Society Wolfson Merit Award. Dr. Yue Wang acknowledges a Research Fellowship awarded by the Royal Academy of Engineering. We also thank Dr. Peter O'Toole, Joanne Marrison, Karen Hogg, Karen Hodgkinson, Graeme Park at the Bioscience Technology Facility at the University of York for their valuable assistance with the confocal microscopy, and Dr. Donato Conteduca, Dr. Giampaolo Pitruzzello for the thoughtful discussions.

AUTHOR CONTRIBUTIONS

Y.W., M.V.D.W. and T.F.K. contributed to the conceptualisation of the experiment; Y.W., C.P.R., N.R. and S.T. carried out the experiments; Y.W. and C.P.R. performed the data analysis; Y.W., A.E., N.T., M.V.D.W. and T.F.K. contributed to the methodology and validation of the experiment; Y.W., C.P.R., N.R., S.T., M.V.D.W. and T.F.K. wrote the manuscript.

COMPETING INTERESTS

The authors declare no competing interests.

ADDITIONAL INFORMATION

Supplementary information is available for this paper at https://doi.org/10.1038/s41522-020-00169-1.

Correspondence and requests for materials should be addressed to Y.W.

Reprints and permission information is available at http://www.nature.com/reprints

Publisher's note Springer Nature remains neutral with regard to jurisdictional claims in published maps and institutional affiliations.